Spontaneously vectorized Einstein-Gauss-Bonnet black holes

Simon Barton [a], Betti Hartmann [b,c,d,e], Burkhard Kleihaus [d,*], Jutta Kunz [d]

[a] *Faculty of Mathematics and Natural Sciences, University of Cologne, D-50923 Cologne, Germany*
[b] *Instituto de Física de São Carlos, Universidade de São Paulo, São Carlos, São Paulo, 13560-970, Brazil*
[c] *Department of Physics and Earth Sciences, Jacobs University Bremen, 28759 Bremen, Germany*
[d] *Institute of Physics, University of Oldenburg, D-26111 Oldenburg, Germany*
[e] *Department of Mathematics, University College London, Gower Street, London, WC1E 6BT, UK*

A B S T R A C T

We construct spontaneously vectorized black holes where a real vector field is coupled to the Gauss-Bonnet invariant. We employ three coupling functions for the vector field, and determine the respective domains of existence of the vectorized black holes. These domains of existence are bounded by the marginally stable Schwarzschild black holes and the critical vectorized black holes. We also address the effects of a mass term. For a given black hole mass the horizon radius is smaller for the vectorized black holes than for the Schwarzschild black holes. Since the vector field vanishes at the horizon, there is no contribution from the Gauss-Bonnet term to the entropy of the vectorized black holes.

1. Introduction

Black holes in General Relativity (GR) satisfy uniqueness theorems [1]. The Schwarzschild and Kerr black holes represent the static, respectively stationary rotating, black hole solutions of the Einstein equations in vacuum. When a real scalar field is admitted, the Schwarzschild and Kerr black holes remain the only black hole solutions: Schwarzschild and Kerr black holes in GR carry no real scalar hair (see e.g., [2]). Inclusion of a massless vector field, however, leads to the Reissner-Nordström and Kerr-Newman black holes of Einstein-Maxwell theory, for which again uniqueness theorems hold [1].

When going beyond GR black holes may carry real scalar fields. For instance, GR may be amended by higher curvature terms, that are coupled to a scalar field. A particular higher curvature term is the Gauss-Bonnet (GB) invariant, whose presence is well-motivated from quantum gravity considerations [3–5]. Moreover, the resulting Einstein-scalar-Gauss-Bonnet (EsGB) theories possess second order field equations and thus avoid Ostrogradski instability and ghosts [6–8].

The coupling of the scalar field to the GB invariant represents a non-minimal coupling, where the coupling function can be chosen freely. A string theory motivated dilatonic coupling function leads to black holes, which are always scalarized [9–21] (see also [22,23]). In this case, the scalar field equation always has a non-vanishing source term, since the derivative of the coupling function with respect to the scalar field is always finite. Therefore the Schwarzschild and Kerr black holes are no longer solutions of the coupled set of EsGB equations.

However, the coupling function can also be chosen to allow for the Schwarzschild and Kerr black holes to be solutions of the coupled set of EsGB equations. In this case the derivative of the coupling function with respect to the scalar field should vanish for some value of the scalar field, such that the scalar field can be chosen to have this constant value throughout. While the Schwarzschild and Kerr black holes remain solutions of the EsGB equations, they do not remain the only solutions, since spontaneously scalarized black hole solutions arise as well [24–45] (see also [46–50]).

In this case, Schwarzschild and Kerr black holes remain solutions of the EsGB equations independent of the value of the GB coupling constant. However, they lose their stability when scalarization sets in. In particular, the GB invariant leads to a tachyonic instability, since it features in the scalar field equation like an effective mass. At a certain threshold value of the GB coupling constant, the GR black holes then develop a zero mode, where a branch of scalarized EsGB black holes emerges. The first zero mode gives rise to the fundamental branch of scalarized black holes, while the next zero modes give rise to radially and angularly excited scalarized black holes. Depending on the coupling function,

* Corresponding author.
E-mail addresses: barton@ph1.uni-koeln.de (S. Barton), betti.hartmann@uni-oldenburg.de (B. Hartmann), b.kleihaus@uni-oldenburg.de (B. Kleihaus), jutta.kunz@uni-oldenburg.de (J. Kunz).

the fundamental scalarized mode may be (at least in part) stable or unstable [24–45].

Spontaneous scalarization of Reissner-Nordström (RN) and Kerr-Newman black holes can be achieved in GR, when the scalar field is non-minimally coupled to the Maxwell invariant with an appropriate coupling function [51–63]. Here the finite value of the Maxwell invariant of a charged black hole provides the effective mass term necessary for the tachyonic instability of the GR black holes. However, for particular choices of coupling functions, also scalarized black hole can arise and coexist with the GR black holes without a tachyonic instability of the GR black holes ever occurring [58,64–66].

However, besides spontaneous scalarization of black holes also spontaneous vectorization of black holes may occur, as argued vigorously by Ramazanoğlu [67–70] (see also [71]). In this case a vector field has to be coupled to an invariant with a suitable coupling function. The black holes of GR then remain solutions of the generalized set of field equations, but succumb to a tachyonic instability induced by the contribution from the invariant in the vector field equation acting as an effective mass. Recently such spontaneously vectorized black hole solutions have been obtained in GR, where an additional vector field has been non-minimally coupled to the Maxwell invariant with an appropriate coupling function [72].

Here we construct and investigate spontaneously vectorized black hole solutions of Einstein-vector-Gauss-Bonnet (EvGB) theories. We employ several coupling functions, which all satisfy the criteria for spontaneous vectorization: they are functions of the vector field squared, $A_\mu A^\mu$, where for a vanishing vector field the coupling functions vanish, allowing the Schwarzschild black hole solutions to remain solutions of the EvGB equations. Since the GB term enters the vector field equations like an effective mass term, a tachyonic instability of the GR black holes results, giving rise to branches of vectorized black holes.

We have organized the paper as follows: Section 2 describes the theoretical setting with the action, the equations of motion, and the boundary conditions, and we define the physical properties. Section 3 contains our physical results, together with a brief description of the numerics. Here we discuss the solutions, the domain of existence and the physical properties of the black holes. We give our conclusions in section 4.

2. Theoretical setting

2.1. Action and equations of motion

We consider the effective action for EvGB theories

$$S = \frac{1}{16\pi} \int \left[R - F_{\mu\nu}F^{\mu\nu} - V(A_\mu A^\mu) + F(A_\mu A^\mu)R_{\text{GB}}^2 \right] \times \sqrt{-g}\, d^4x \,, \tag{1}$$

where R is the curvature scalar, and $F_{\mu\nu}$ denotes the field strength tensor of the real vector field A_μ with potential $V(A_\mu A^\mu)$. The vector field is coupled with some coupling function $F(A_\mu A^\mu)$ to the Gauss-Bonnet term

$$R_{\text{GB}}^2 = R_{\mu\nu\rho\sigma}R^{\mu\nu\rho\sigma} - 4R_{\mu\nu}R^{\mu\nu} + R^2 \,. \tag{2}$$

For the coupling function $F(A_\mu A^\mu)$ we make the following choices

$$F(A_\mu A^\mu) = \begin{cases} \lambda\left(1 - e^{-\beta A_\mu A^\mu}\right) & (i) \\ \lambda\left(e^{\beta A_\mu A^\mu} - 1\right) & (ii) \\ \lambda A_\mu A^\mu & (iii) \end{cases} \tag{3}$$

with coupling constants λ and β. When the vector field vanishes, $A_\mu = 0$, all three coupling functions reduce to zero. The potential $V(A_\mu A^\mu)$

$$V(A_\mu A^\mu) = 2m_A^2 A_\mu A^\mu - 2\alpha\left(A_\mu A^\mu\right)^2 \tag{4}$$

has a mass term with vector field mass m_A and a self-interaction with coupling constant α. We here mostly focus on $\alpha = 0$. While the Gauss-Bonnet invariant R_{GB}^2 itself is topological in four dimensions, its coupling to the vector field A_μ by means of the coupling function $F(A_\mu A^\mu)$ leads to significant contributions to the equations of motion.

The coupled set of field equations follows from the variational principle. Variation of the action (1) with respect to the vector field and the metric yields the Proca equation and the Einstein equations

$$\nabla_\mu F^{\mu\nu} = \frac{1}{2}\frac{dV(A_\mu A^\mu)}{d(A_\mu A^\mu)}A^\nu - \frac{1}{2}\frac{dF(A_\mu A^\mu)}{d(A_\mu A^\mu)}R_{\text{GB}}^2 A^\nu \,, \tag{5}$$

$$G_{\mu\nu} = \frac{1}{2}T_{\mu\nu}^{(\text{eff})} \,, \tag{6}$$

where $G_{\mu\nu}$ is the Einstein tensor and $T_{\mu\nu}^{(\text{eff})}$ denotes the effective stress-energy tensor

$$T_{\mu\nu}^{(\text{eff})} = T_{\mu\nu}^{(A)} - 2T_{\mu\nu}^{(GB)} \,, \tag{7}$$

which consists of a contribution from the vector field

$$\begin{aligned} T_{\mu\nu}^{(A)} =& 4F_\mu{}^\lambda F_{\nu\lambda} \\ &+ 2\frac{dV(A_\lambda A^\lambda)}{d(A_\lambda A^\lambda)}A_\mu A_\nu - g_{\mu\nu}\left(F_{\rho\lambda}F^{\rho\lambda} + V(A_\lambda A^\lambda)\right) \,, \end{aligned} \tag{8}$$

and a contribution from the GB term R_{GB}^2

$$\begin{aligned} T_{\mu\nu}^{(GB)} =& \frac{1}{2}\left(g_{\rho\mu}g_{\lambda\nu} + g_{\lambda\mu}g_{\rho\nu}\right)\eta^{\kappa\lambda\alpha\beta}\tilde{R}^{\rho\gamma}{}_{\alpha\beta}\nabla_\gamma\nabla_\kappa F(A_\mu A^\mu) \\ &+ R_{\text{GB}}^2\frac{dF(A_\sigma A^\sigma)}{d(A_\sigma A^\sigma)}A_\mu A_\nu \,, \end{aligned} \tag{9}$$

where $\tilde{R}^{\rho\gamma}{}_{\alpha\beta} = \eta^{\rho\gamma\sigma\tau}R_{\sigma\tau\alpha\beta}$ and $\eta^{\rho\gamma\sigma\tau} = \epsilon^{\rho\gamma\sigma\tau}/\sqrt{-g}$. Note that the last term results from the dependence of the coupling function on the metric.

To obtain static, spherically symmetric black holes we employ isotropic coordinates for the line element

$$ds^2 = -F_0 dt^2 + e^{f_1}\left[dr^2 + r^2\left(d\theta^2 + \sin^2\theta\, d\varphi^2\right)\right] \,, \tag{10}$$

and we assume for the vector field the form

$$A_\mu dx^\mu = A_t dt \,. \tag{11}$$

All three functions, the two metric functions F_0 and f_1 and the vector field function A_t, depend only on the radial coordinate r.

When we insert the above ansatz (10)-(11) for the metric and the vector field into the set of EvGB equations we obtain five coupled, nonlinear ordinary differential equations (ODEs). However, these are not independent, two of the Einstein equations are equivalent due to spherical symmetry, and one ODE can be treated as a constraint. This leaves us with three second order ODEs. We note that the choice of Schwarzschild-like coordinates results in second order ODEs with very lengthy expressions [24], whereas the choice of isotropic coordinates leads to Einstein and vector field equations which are linear in the second derivatives.

Inspection of the field equations reveals an invariance under the scaling transformation

$$r \to \chi r \,, \quad t \to \chi t \,, \quad F \to \chi^2 F \,, \quad V \to V/\chi^2 \,, \quad \chi > 0 \,. \tag{12}$$

2.2. Black hole properties

We are looking for vectorized black holes with a regular horizon. Inspecting the equations of motion for the functions, and performing an expansion at the horizon leads to

$$F_0(r) = F_{02} \left(\frac{r - r_H}{r_H} \right)^2 + O \left(\frac{r - r_H}{r_H} \right)^3 , \qquad (13)$$

$$f_1(r) = f_1(r_H) + O \left(\frac{r - r_H}{r_H} \right) , \qquad (14)$$

$$A_t(r) = A_{t2} \left(\frac{r - r_H}{r_H} \right)^2 + O \left(\frac{r - r_H}{r_H} \right)^3 , \qquad (15)$$

with constants F_{02}, $f_1(r_H)$, and A_{t2}. Thus at the horizon the metric function F_0 vanishes, while f_1 is finite. Interestingly, also the vector field function A_t vanishes at the horizon, but $A^t(r = r_H) = A_{t2}/F_{02}$ is finite.

To address the physical properties of the vectorized black holes at the horizon we note that the metric of a spatial cross-section of the horizon is

$$d\Sigma_H^2 = h_{ij} dx^i dx^j = r_H^2 e^{f_1(r_H)} \left(d\theta^2 + \sin^2\theta d\varphi^2 \right) . \qquad (16)$$

The horizon area of the black holes is then given by

$$A_H = 4\pi r_H^2 e^{f_1(r_H)}. \qquad (17)$$

In GR the entropy is simply a quarter of the horizon area [73], but this may no longer be the case in the presence of a GB term. In the case of scalarized black holes the entropy of black holes acquires an additional contribution due to the coupling to the GB term [74–79]. For vectorized black holes an analogous additional term arises, and the entropy can be expressed as the following integral over the horizon

$$S = \frac{1}{4} \int_{\Sigma_H} d^2 x \sqrt{h} \left[1 + 2F(A_\mu A^\mu) \tilde{R} \right], \qquad (18)$$

where h is the determinant of the induced metric on the horizon, Eq. (16), and $\tilde{R}$ is the horizon curvature. Since, however, the vector field function A_t vanishes at the horizon, also the chosen coupling functions (i)-(iii) vanish at the horizon. Therefore we obtain no contribution from the GB term to the entropy, and the entropy remains equal to a quarter of the horizon area,

$$S = \frac{A_H}{4}. \qquad (19)$$

The Killing vector field $\chi = \partial_t$ determines the surface gravity κ [73], where $\kappa^2 = -\frac{1}{2}(\nabla_a \chi_b)(\nabla^a \chi^b)|_{r_H}$, yielding the Hawking temperature $T_H = \kappa/(2\pi)$

$$T_H = \frac{1}{2\pi r_H} \sqrt{F_{02}} e^{-f_1(r_H)/2}. \qquad (20)$$

We require the black hole solutions to be asymptotically flat. From the expansion at radial infinity

$$g_{tt} = -1 + \frac{2M}{r} + \dots , \qquad (21)$$

$$g_{rr} = 1 + \frac{2M}{r} + \dots , \qquad (22)$$

$$A_t = \frac{\tilde{Q}}{r} e^{-m_A r} + \dots . \qquad (23)$$

with constants M and $\tilde{Q}$, we determine the asymptotic boundary conditions for the functions

$$F_0(\infty) = 1, \quad f_1(\infty) = 0, \quad A_t(\infty) = 0 . \qquad (24)$$

The constant M in the expansion corresponds to the total mass of the black hole solutions. This value agrees with the Komar mass, when the Komar integral is evaluated at spatial infinity. When the Komar integral is evaluated at the horizon, the horizon mass M_H is obtained. For Schwarzschild black holes the horizon mass M_H is identical to the total mass M. For vectorized black holes this is no longer the case, since the total mass M receives a contribution from the bulk.

We define a vector charge Q by the integral expression

$$Q = \frac{1}{4\pi} \int \sqrt{-g} F^{rt} \big|_{r \to \infty} d\theta d\varphi = Q_H + \frac{1}{4\pi} \int_{r > r_H} \sqrt{-g} j^t d^3 x \quad (25)$$

with the time component of the current density $j^\nu = \nabla_\mu F^{\mu\nu}$, and the horizon charge Q_H

$$Q_H = \frac{1}{4\pi} \int \sqrt{-g} F^{rt} \big|_{r = r_H} d\theta d\varphi . \qquad (26)$$

In the case of a massless vector field the vector charge Q coincides with the constant $\tilde{Q}$, Eq. (23), whereas in the case of a massive vector field the charge vanishes at radial infinity, $Q = 0$. The horizon charge Q_H, on the other hand, remains finite for massless and massive vector fields.

3. Results

3.1. Numerics

In order to solve the set of coupled Einstein and vector field equations numerically we introduce the radial coordinate

$$x = 1 - \frac{r_H}{r} , \qquad (27)$$

to compactify the domain of integration, $0 \le x \le 1$.

The expansions close to the horizon, Eqs. (13) and (15) suggest a factorization of the double-zeros of the functions F_0 and A_t,

$$F_0(x) = x^2 f_0(x) , \quad A_t(x) = x^2 b(x) . \qquad (28)$$

Expansion of the Einstein and vector field equations close to $x = 0$ then yields the boundary conditions at the horizon ($x = 0$)

$$f_0'(0) - f_0(0) = 0 , \quad f_1'(0) = 2 , \quad b_0'(0) - b(0) = 0 , \qquad (29)$$

whereas the boundary conditions in the asymptotic region ($x = 1$) are obtained from Eqs. (24),

$$f_0(1) = 1 , \quad f_1(1) = 0 , \quad b(1) = 0 . \qquad (30)$$

We then employ the professional solver COLSYS [80]. COL-SYS uses a collocation method to solve systems of boundary-value ODEs with the help of a damped Newton method of quasi-linearization and an adaptive mesh selection procedure. Starting from an initial guess, the iteration process then proceeds with successively refined grids until a specified accuracy of the functions is reached. The prescribed tolerances are typically of the order 10^{-5}, but the numerical error estimates are even smaller. When calculating the solutions we fix the isotropic horizon coordinate $r_H = 1$, and thus break the scale invariance, Eqs. (12).

3.2. Solutions

We exhibit some typical vectorized black hole solutions in Fig. 1. The figures show the metric functions F_0 and f_1 together with the vector field function A_t versus the compactified radial coordinate x, Eq. (27), for the coupling functions (i) and (ii) and
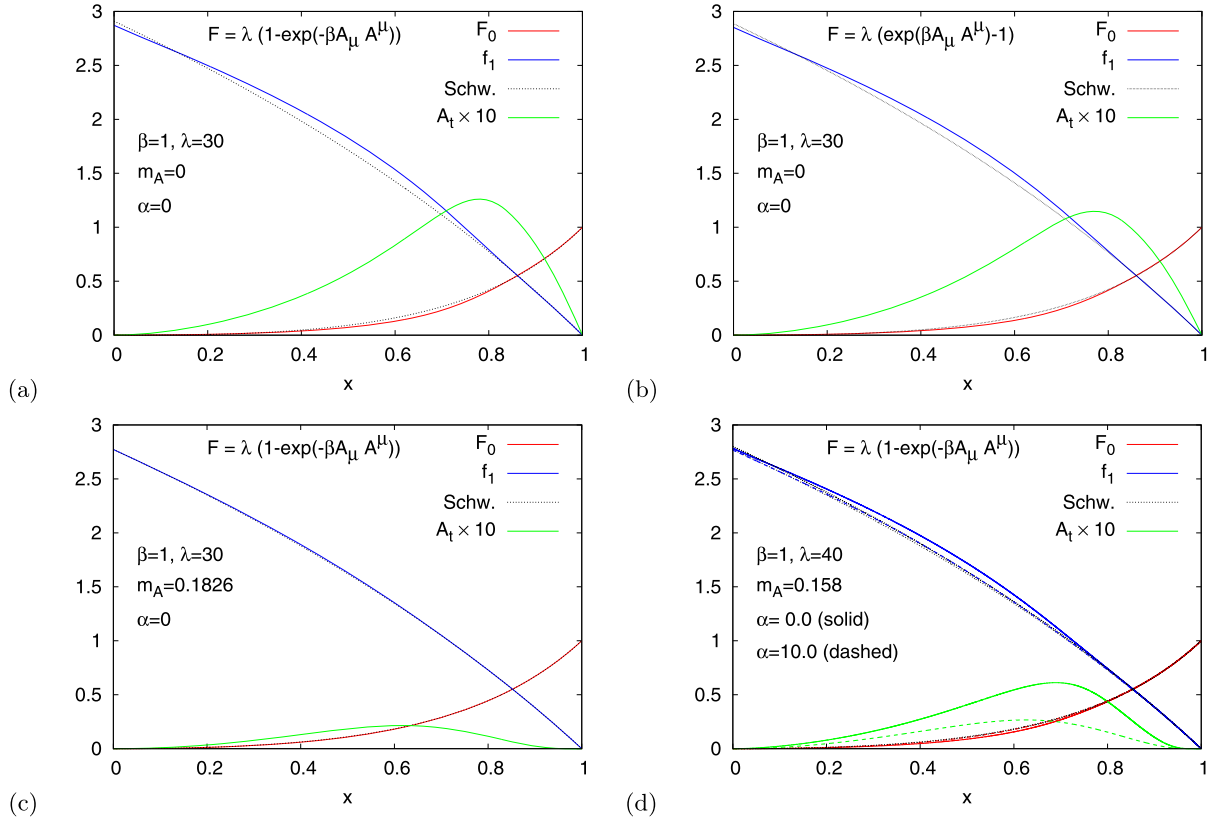
Fig. 1. Examples of vectorized black hole solutions: metric functions F_0, f_1, and vector field function A_t vs compactified radial coordinate x for (a) coupling function (i) and parameters $\lambda = 30$, $\beta = 1$, $m_A = 0$, $\alpha = 0$; (b) coupling function (ii) and parameters $\lambda = 30$, $\beta = 1$, $m_A = 0$, $\alpha = 0$; (c) coupling function (i) and parameters $\lambda = 30$, $\beta = 1$, $m_A = 0.1826$, $\alpha = 0$; (d) coupling function (i) and parameters $\lambda = 40$, $\beta = 1$, $m_A = 0.158$, $\alpha = 0$ (solid) and $\alpha = 10$ (dashed). Note the Schwarzschild metric functions (thin-dotted) for comparison.

selected values of the coupling constants and the potential parameters. The vector field function exhibits a pronounced maximum at several times the horizon radius. This maximum decreases in size and shifts to smaller radii as the vector field mass and self-interaction are increased. In all cases, the metric functions of the vectorized black holes deviate only somewhat from the Schwarzschild metric functions, with the deviation decreasing as the vector field mass and self-interaction are increased.

We illustrate the components $T_t^{t(\text{eff})}$, $T_r^{r(\text{eff})}$, and $T_\theta^{\theta(\text{eff})}$ of the effective stress-energy tensor versus the compactified radial coordinate x in Fig. 2 for the same set of solutions. We note, that at the horizon

$$T_t^{t(\text{eff})}(r_\text{H}) = T_r^{r(\text{eff})}(r_\text{H}) = 4\frac{b_\text{H}^2}{\rho_\text{H}^2 f_{0\text{H}}^2}(2l_\text{H} - 1) \ , \tag{31}$$

$$T_\theta^{\theta(\text{eff})}(r_\text{H}) = -T_t^t(r_\text{H})\frac{f_{0\text{H}} + 8l_\text{H}b_\text{H}^2}{f_{0\text{H}}} \ , \tag{32}$$

where we have introduced the circumferential horizon radius $\rho_\text{H} = e^{f_{1,\text{H}}/2}r_\text{H}$, and $f_{0\text{H}} = f_0(r_\text{H})$, $b_\text{H} = b(r_\text{H})$, and $l_\text{H} = \beta\lambda/\rho_\text{H}^2$ for (i) and (ii), while $l_\text{H} = \lambda/\rho_\text{H}^2$ for (iii). Since $-T_t^{t(\text{eff})}$ can be interpreted as an effective energy density, Eq. (31) shows that near the horizon the effective energy density is negative. Somewhat away from the horizon the effective energy density then turns positive, only to become negative again when the vector field function approaches its maximum. Although the effective energy density exhibits this oscillating behaviour, the contribution to the mass from the region outside the horizon is in all cases positive.

3.2.1. Domain of existence: massless case

We now address the domain of existence of the vectorized black holes for vanishing potential V. The domain of existence is illustrated in Fig. 3 for all three coupling functions, where we have set the second coupling constant β to $\beta = 1$ for the cases (i) and (ii). We show in Fig. 3(a) the vector charge Q^2/λ versus the black hole mass M^2/λ, where we have scaled with the coupling constant λ. For comparison we show in Fig. 3(b) the vector charge Q/M versus the coupling constant λ/M^2, where we have scaled with the black hole mass M.

We note, that independent of the coupling function, the branches of vectorized black holes emerge from the Schwarzschild solution at $M^2/\lambda = 0.2136$, where the tachyonic instability of the Schwarzschild solution sets in, manifesting in a zero mode of the Schwarzschild solution. The branches then extend to smaller values of M^2/λ. Here the effect of the coupling function becomes important, and we note, that the vector charge Q/M is largest for the coupling function (i), and smallest for the coupling function (ii). The branches finally end at critical solutions, when M^2/λ tends to zero. At these critical solutions a curvature singularity is encountered at the horizon.

To analyze the critical behaviour we consider the Ricci scalar and the GB invariant at the horizon, R_H and $R_{\text{GB}\,\text{H}}^2$, respectively, and scale these with the square of the circumferential horizon radius ρ_H, to obtain scale-invariant expressions. Analytic expressions for these scaled curvature invariants at the horizon are then given by

$$\rho_\text{H}^2 R_\text{H} = \frac{64b_\text{H}^4}{f_{0\text{H}}^2}l_\text{H}(2l_\text{H} - 1) \ ,$$
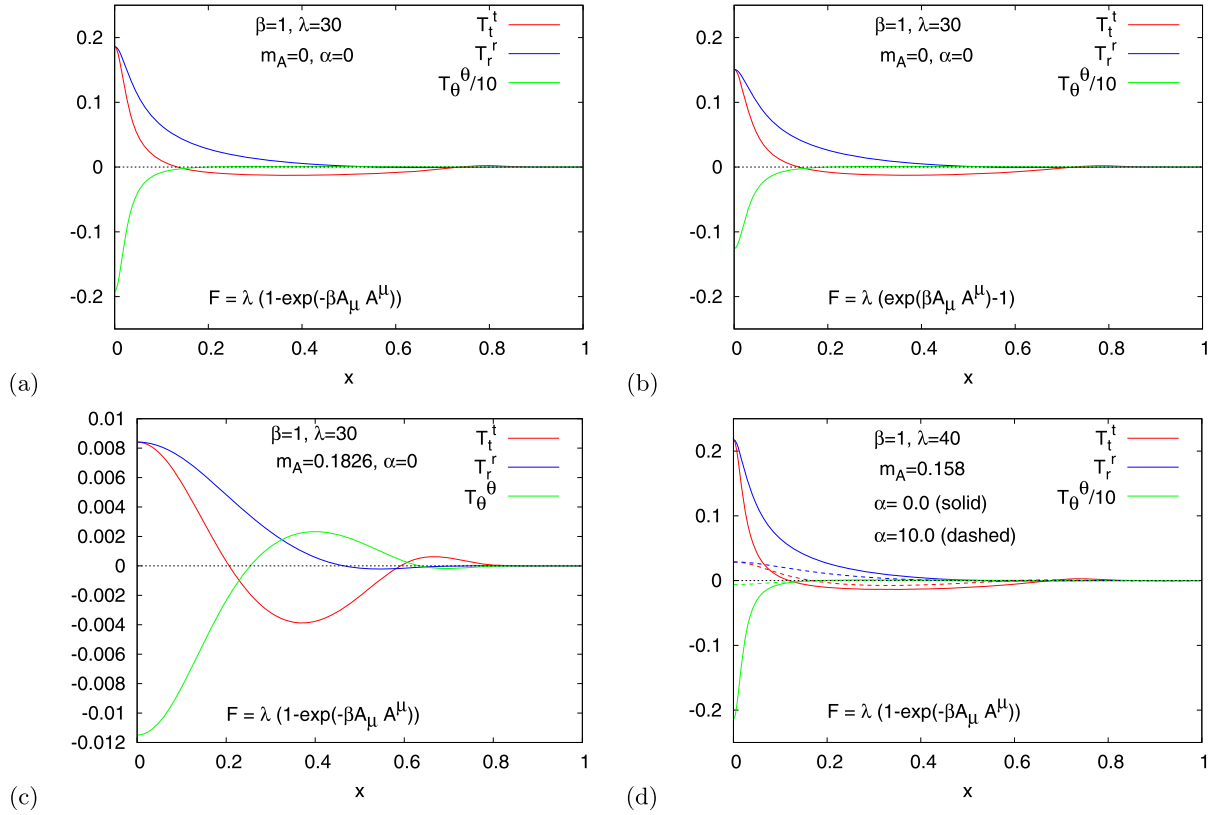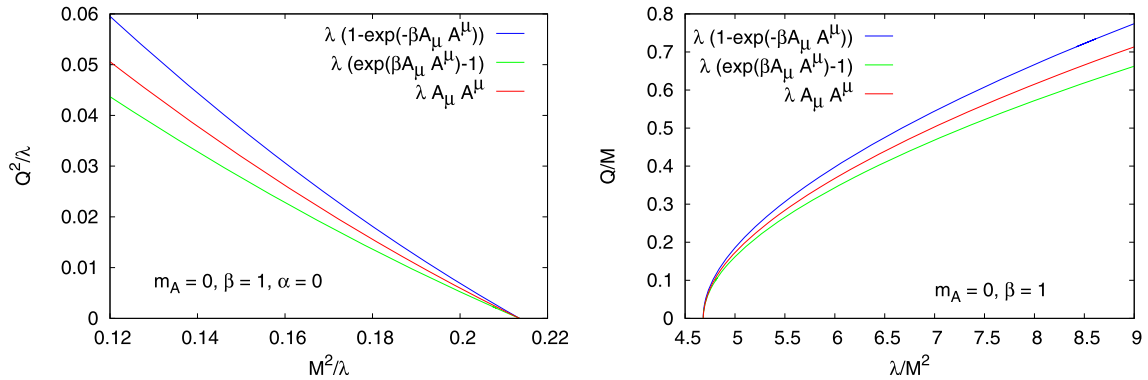
Fig. 2. Examples of vectorized black hole solutions: effective stress-energy tensor components $T_t^{t(\text{eff})}$, $T_r^{r(\text{eff})}$, and $T_\theta^{\theta(\text{eff})}$ vs compactified radial coordinate x for (a) coupling function (i) and parameters $\lambda = 30$, $\beta = 1$, $m_A = 0$, $\alpha = 0$; (b) coupling function (ii) and parameters $\lambda = 30$, $\beta = 1$, $m_A = 0$, $\alpha = 0$; (c) coupling function (i) and parameters $\lambda = 30$, $\beta = 1$, $m_A = 0.1826$, $\alpha = 0$; (d) coupling function (i) and parameters $\lambda = 40$, $\beta = 1$, $m_A = 0.158$, $\alpha = 0$ (solid) and $\alpha = 10$ (dashed).

Fig. 3. Domain of existence for all three coupling functions ($V = 0$): (a) vector charge Q^2/λ vs black hole mass M^2/λ; (b) vector charge Q/M vs coupling constant λ/M^2.

$$\rho_H^4 R_{\text{GBH}}^2 = \frac{4}{f_{0H}^2} \left\{ 16 b_H^4 (2l_H - 1)(6l_H - 1) \right.$$
$$\left. + 3 \left[8(2l_H - 1) b_H^2 + f_{0H} \right] f_{0H} \right\}, \quad (33)$$

in the notation of Eqs. (31)-(32). Note that these expressions are independent of the potential $V(A_\mu A^\mu)$.

We demonstrate the critical behaviour in Fig. 4 for the coupling function (i), where we show the scaled Ricci scalar $\rho_H^2 R_H$ and the scaled GB invariant $\rho_H^2 R_{\text{GBH}}^2$ at the horizon as functions of the scaled coupling parameter $l_H = \beta \lambda / \rho_H^2$. We observe that these scaled curvature invariants increase exponentially with l_H and reach very large values already for moderate values of l_H.

As in the case of scalarization, there are also excited vectorized black hole solutions. Here we only note that independent of the coupling function the branches of vectorized black holes with a

single node arise at $M^2/\lambda = 0.00598$. This is to be compared to the onset of the fundamental branches of vectorized solutions at $M^2/\lambda = 0.2136$. We expect a countable number of higher excited solutions, arising at successively smaller values of M^2/λ.

We now turn to the horizon properties and define the reduced horizon area a_H and the reduced temperature t_H

$$a_H = \frac{A_H}{16\pi}, \quad t_H = 4\pi T_H. \quad (34)$$

We exhibit in Fig. 5(a) the reduced horizon area a_H/M^2 and in Fig. 5(b) the reduced temperature $t_H M$ for all three coupling functions and vanishing potential V versus the coupling constant λ/M^2. For all three coupling functions the area of the vectorized black holes is smaller than for the Schwarzschild black holes, and the area is smallest for the coupling function (i) and largest for
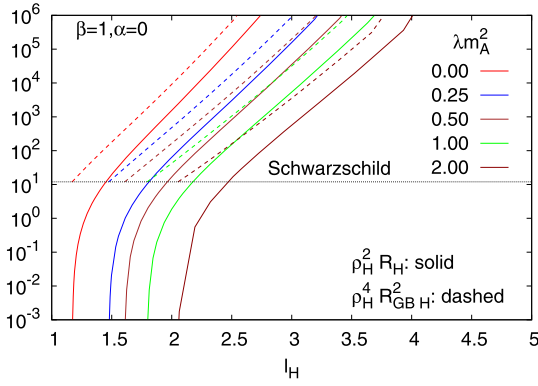
Fig. 4. Curvature invariants at the horizon: scale-invariant curvature invariants $\rho_H^2 R_H$ (solid) and $\rho_H^4 R_{GBH}^2$ (dashed) vs the dimensionless coupling parameter l_H for coupling function (i) and several values of the vector field mass m_A.

(ii). Analogously the temperature of the vectorized black holes is smaller than for the Schwarzschild black holes.

As discussed above, the entropy of these vectorized black holes is simply given by a quarter of their horizon area, since the GB term does not contribute, being multiplied by a coupling function which vanishes at the horizon. Thus we have to conclude from Fig. 5(a) that the Schwarzschild solutions are entropically favored over the vectorized solutions. The reason, that the horizon area and thus the entropy is smaller for the vectorized solutions then stems from the fact that their total mass contains a contribution from the bulk outside the horizon. Therefore, for a given total mass, the horizon radius for a vectorized black hole is smaller than for a Schwarzschild back hole, which is a vacuum solution.

3.2.2. Domain of existence: influence of vector field mass m_A

We next consider the effects of a finite mass m_A of the vector field. The presence of an ordinary finite mass term in the vector field equation (5) clearly affects the effective mass responsible for the tachyonic instability of the Schwarzschild black holes, which now consists of two contributions: the ordinary mass and the curvature-induced mass. Consequently, the value of the coupling constant λ, where the Schwarzschild solution develops a zero mode, changes with the vector field mass m_A. Denoting this coupling constant by λ_{ex}, we thus obtain the existence line for the vectorized black hole solutions $m_A(\lambda_{ex})$.

We exhibit the existence line in Fig. 6. We show the vector field mass m_A/M versus the coupling constant λ_{ex}/M^2 in Fig. 6(a). The figure shows, that the onset of the tachyonic instability of the Schwarzschild black hole is shifted to larger values of λ, when the vector field mass is increased. This is to be expected, since the finite vector field mass increases the effective mass in the vector field equation, which must then be compensated by a larger contribution from the curvature-induced contribution to the effective mass, and this latter contribution is proportional to λ. When considering the vector field mass $\lambda_{ex}^{1/2} m_A$ versus the coupling constant λ_{ex}/M^2, as shown in Fig. 6(b), we obtain basically a linear relation, also demonstrated in the figure by the linear fit.

The existence line depends only on the effective mass in the vector field equation (5) and thus the terms linear in the vector field. Higher powers of the vector field do not matter for the onset of the tachyonic instability. Therefore all three coupling functions possess the same existence line. Similarly, adding self-interaction terms to the potential V will also not affect the existence line. The effect of higher powers in the coupling function or in the potential does of course influence the domain of existence of the vectorized black hole solutions.

We exhibit in Fig. 7 the domain of existence of the vectorized black hole solutions for the coupling functions (i), (ii) and (iii) with

potential $V = 2m_A^2 A_\mu A^\mu$, to illustrate the dependence on the vector field mass m_A. Since the charge Q vanishes for solutions with non-zero vector field mass, we employ the horizon charge Q_H, Eq. (26). Fig. 7(a) shows the horizon charge Q_H^2/λ versus the black hole mass M^2/λ, and Fig. 7(b) the horizon charge Q_H/M versus the coupling constant λ/M^2. Analogously to the case of vanishing vector field mass, the vectorized black hole solutions develop a curvature singularity at the horizon when M^2/λ tends to zero. As noted above, the scaled curvature invariants at the horizon, Eqs. (33), are independent of the potential $V(A_\mu A^\mu)$. The dependence of the scaled curvature invariants on the vector field mass m_A is seen in Fig. 4.

We illustrate the dependence of the horizon properties on the vector field mass m_A in Fig. 8 for the coupling functions (i), (ii) and (iii) with potential $V = 2m_A^2 A_\mu A^\mu$. The reduced horizon area a_H/M^2 is shown in Fig. 8(a) and the reduced temperature $t_H M$ in Fig. 8(b). We note that also in the presence of a finite vector field mass m_A the horizon area of the vectorized black holes is smaller than for the Schwarzschild black holes, and the area is smallest for the coupling function (i) and largest for (ii). But the area a_H/M^2 decreases less rapidly with increasing λ/M^2, when the vector field mass increases. The temperature exhibits a similar dependence on the vector field mass.

Since the entropy of these vectorized black holes is simply given by a quarter of their horizon area, independent of the potential V, we conclude from Fig. 8(a) that as in the massless case the Schwarzschild black holes are entropically favored over the vectorized black holes, independent of the employed coupling function.

4. Conclusions

Here we have performed a first exploratory study of curvature-induced spontaneously vectorized black holes. These novel black holes arise when a vector field is coupled to the GB term by employing a coupling function that is quadratic in the vector field. The GB term then induces a tachyonic instability of the Schwarzschild black holes, which start to grow vector hair.

We have allowed for three different types of coupling functions in order to see their basic influence. However, unlike the case of curvature-induced spontaneously scalarized black holes, we did not observe distinctly different physical properties of the vectorized black holes for these coupling functions. In particular, for all coupling functions the branches of vectorized black holes extend from their bifurcation point to smaller values of the scaled coupling constant M^2/λ.

The bifurcation point does not depend on the coupling function. However it does depend on the mass of the vector field. With increasing mass the bifurcation point shifts to larger values of the coupling constant, while it is not affected by vector field self-interactions. Radially excited spontaneously vectorized black holes also exist. Their bifurcation points are at smaller values of M^2/λ than the bifurcation point of the fundamental branch of vectorized black holes.

We have shown that independent of the coupling function and the vector field potential V, all fundamental branches extend to $M^2/\lambda \to 0$, where the vectorized black holes develop a curvature singularity at the horizon. The scaled Ricci scalar and the scaled GB invariant exhibit an exponential dependence on the scaled coupling parameter, which results in a divergence in the limit.

We have also addressed some thermodynamic properties of the vectorized black holes. In particular, we have calculated the horizon temperature, the horizon area and the entropy. Along the branches of vectorized black holes the scaled temperature and the scaled entropy decrease monotonically with increasing coupling constant from the Schwarzschild values at the bifurcation. Thus for a given mass, the vectorized black holes have smaller area than
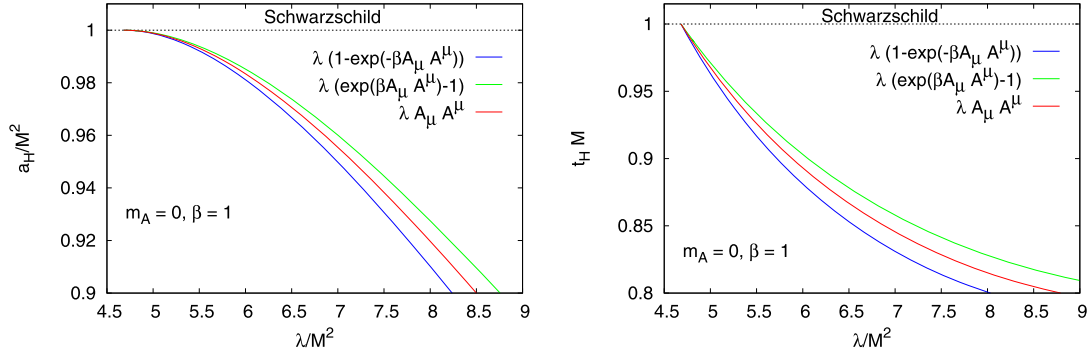
Fig. 5. Horizon properties for all three coupling functions ($V = 0$): (a) reduced horizon area a_H/M^2 vs coupling constant λ/M^2; (b) reduced temperature $t_H M$ vs coupling constant λ/M^2.
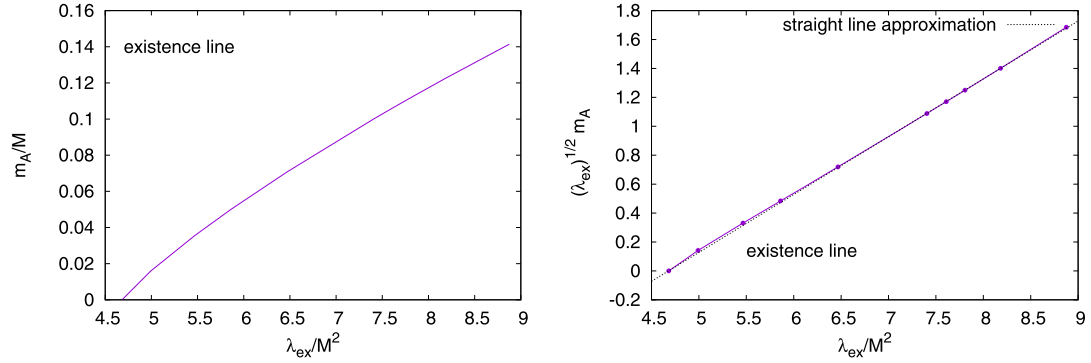

Fig. 6. Existence line: (a) vector field mass m_A/M vs coupling constant λ_{ex}/M^2; (b) vector field mass $\lambda_{ex}^{1/2} m_A$ vs coupling constant λ_{ex}/M^2 (solid) together with a linear fit (dotted).
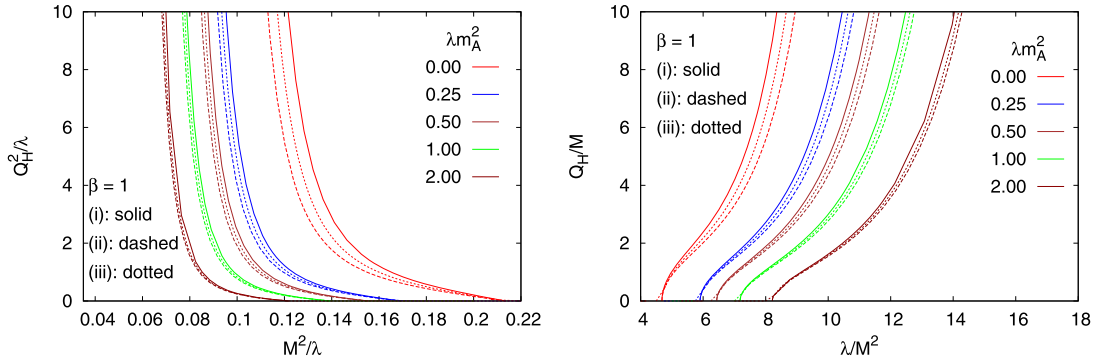

Fig. 7. Domain of existence for coupling functions (i), (ii) and (iii) ($V = 2m_A^2 A_\mu A^\mu$) for several values of λm_A^2: (a) vector charge Q_H^2/λ vs black hole mass M^2/λ; (b) vector charge Q_H/M vs coupling constant λ/M^2.
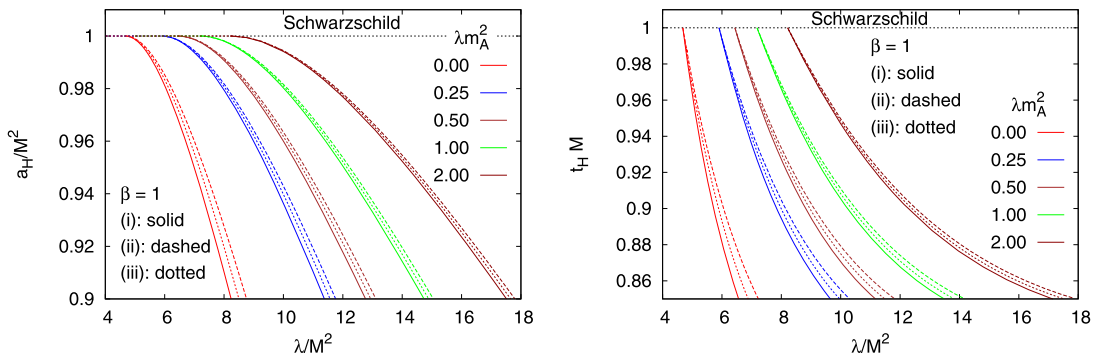

Fig. 8. Horizon properties for coupling functions (i), (ii) and (iii) ($V = 2m_A^2 A_\mu A^\mu$) for several values of λm_A^2: (a) reduced horizon area a_H/M^2 vs coupling constant λ/M^2; (b) reduced temperature $t_H M$ vs coupling constant λ/M^2.

the Schwarzschild black holes. Since the GB term of the vectorized black holes does not contribute to their entropy, this entails that Schwarzschild black holes are entropically preferred.

There are various interesting directions to continue these investigations. These include foremost a mode analysis of the static spherically symmetric vectorized black holes and a generalization to the rotating case. But also a further analysis of the physical properties is called for, ranging from a study of their geodesics and lightrings to their accretion discs.

Declaration of competing interest

The authors declare that they have no known competing financial interests or personal relationships that could have appeared to influence the work reported in this paper.

Acknowledgement

References

[1] P.T. Chrusciel, J. Lopes Costa, M. Heusler, Living Rev. Relativ. 15 (2012) 7.
[2] C.A.R. Herdeiro, E. Radu, Int. J. Mod. Phys. D 24 (09) (2015) 1542014.
[3] B. Zwiebach, Phys. Lett. B 156 (1985) 315.
[4] D.J. Gross, J.H. Sloan, Nucl. Phys. B 291 (1987) 41.
[5] R.R. Metsaev, A.A. Tseytlin, Nucl. Phys. B 293 (1987) 385.
[6] G.W. Horndeski, Int. J. Theor. Phys. 10 (1974) 363.
[7] C. Charmousis, E.J. Copeland, A. Padilla, P.M. Saffin, Phys. Rev. Lett. 108 (2012) 051101.
[8] T. Kobayashi, M. Yamaguchi, J. Yokoyama, Prog. Theor. Phys. 126 (2011) 511.
[9] P. Kanti, N.E. Mavromatos, J. Rizos, K. Tamvakis, E. Winstanley, Phys. Rev. D 54 (1996) 5049.
[10] T. Torii, H. Yajima, K.i. Maeda, Phys. Rev. D 55 (1997) 739.
[11] Z.K. Guo, N. Ohta, T. Torii, Prog. Theor. Phys. 120 (2008) 581.
[12] P. Pani, V. Cardoso, Phys. Rev. D 79 (2009) 084031.
[13] P. Pani, C.F.B. Macedo, L.C.B. Crispino, V. Cardoso, Phys. Rev. D 84 (2011) 087501.
[14] B. Kleihaus, J. Kunz, E. Radu, Phys. Rev. Lett. 106 (2011) 151104.
[15] D. Ayzenberg, K. Yagi, N. Yunes, Phys. Rev. D 89 (4) (2014) 044023.
[16] D. Ayzenberg, N. Yunes, Phys. Rev. D 90 (2014) 044066.
[17] A. Maselli, P. Pani, L. Gualtieri, V. Ferrari, Phys. Rev. D 92 (8) (2015) 083014.
[18] B. Kleihaus, J. Kunz, S. Mojica, Phys. Rev. D 90 (6) (2014) 061501.
[19] B. Kleihaus, J. Kunz, S. Mojica, E. Radu, Phys. Rev. D 93 (4) (2016) 044047.
[20] J.L. Blázquez-Salcedo, C.F.B. Macedo, V. Cardoso, V. Ferrari, L. Gualtieri, F.S. Khoo, J. Kunz, P. Pani, Phys. Rev. D 94 (10) (2016) 104024.
[21] J.L. Blázquez-Salcedo, F.S. Khoo, J. Kunz, Phys. Rev. D 96 (6) (2017) 064008.
[22] T.P. Sotiriou, S.Y. Zhou, Phys. Rev. Lett. 112 (2014) 251102.
[23] T.P. Sotiriou, S.Y. Zhou, Phys. Rev. D 90 (2014) 124063.
[24] G. Antoniou, A. Bakopoulos, P. Kanti, Phys. Rev. Lett. 120 (13) (2018) 131102;
G. Antoniou, A. Bakopoulos, P. Kanti, Phys. Rev. D 97 (8) (2018) 084037.
[25] D.D. Doneva, S.S. Yazadjiev, Phys. Rev. Lett. 120 (13) (2018) 131103.
[26] H.O. Silva, J. Sakstein, L. Gualtieri, T.P. Sotiriou, E. Berti, Phys. Rev. Lett. 120 (13) (2018) 131104.
[27] G. Antoniou, A. Bakopoulos, P. Kanti, Phys. Rev. D 97 (8) (2018) 084037.
[28] J.L. Blázquez-Salcedo, D.D. Doneva, J. Kunz, S.S. Yazadjiev, Phys. Rev. D 98 (8) (2018) 084011.
[29] D.D. Doneva, S. Kiorpelidi, P.G. Nedkova, E. Papantonopoulos, S.S. Yazadjiev, Phys. Rev. D 98 (10) (2018) 104056.
[30] M. Minamitsuji, T. Ikeda, Phys. Rev. D 99 (4) (2019) 044017.
[31] H.O. Silva, C.F.B. Macedo, T.P. Sotiriou, L. Gualtieri, J. Sakstein, E. Berti, Phys. Rev. D 99 (6) (2019) 064011.
[32] Y. Brihaye, L. Ducobu, Phys. Lett. B 795 (2019) 135.
[33] A. Bakopoulos, G. Antoniou, P. Kanti, Phys. Rev. D 99 (6) (2019) 064003.
[34] D.D. Doneva, K.V. Staykov, S.S. Yazadjiev, Phys. Rev. D 99 (10) (2019) 104045.
[35] C.F.B. Macedo, J. Sakstein, E. Berti, L. Gualtieri, H.O. Silva, T.P. Sotiriou, Phys. Rev. D 99 (10) (2019) 104041.
[36] Y.S. Myung, D.C. Zou, Int. J. Mod. Phys. D 28 (09) (2019) 1950114.
[37] P.V.P. Cunha, C.A.R. Herdeiro, E. Radu, Phys. Rev. Lett. 123 (1) (2019) 011101.
[38] A. Bakopoulos, P. Kanti, N. Pappas, Phys. Rev. D 101 (4) (2020) 044026.
[39] S. Hod, Phys. Rev. D 100 (6) (2019) 064039.
[40] L.G. Collodel, B. Kleihaus, J. Kunz, E. Berti, Class. Quantum Gravity 37 (7) (2020) 075018.
[41] A. Bakopoulos, P. Kanti, N. Pappas, Phys. Rev. D 101 (8) (2020) 084059.
[42] J.L. Blázquez-Salcedo, D.D. Doneva, S. Kahlen, J. Kunz, P. Nedkova, S.S. Yazadjiev, Phys. Rev. D 101 (10) (2020) 104006.
[43] J.L. Blázquez-Salcedo, D.D. Doneva, S. Kahlen, J. Kunz, P. Nedkova, S.S. Yazadjiev, Phys. Rev. D 102 (2) (2020) 024086.
[44] C.A.R. Herdeiro, E. Radu, H.O. Silva, T.P. Sotiriou, N. Yunes, Phys. Rev. Lett. 126 (1) (2021) 011103.
[45] E. Berti, L.G. Collodel, B. Kleihaus, J. Kunz, Phys. Rev. Lett. 126 (1) (2021) 011104.
[46] A. Dima, E. Barausse, N. Franchini, T.P. Sotiriou, Phys. Rev. Lett. 125 (23) (2020) 231101.
[47] S. Hod, Phys. Rev. D 102 (8) (2020) 084060.
[48] D.D. Doneva, L.G. Collodel, C.J. Krüger, S.S. Yazadjiev, Phys. Rev. D 102 (2020) 104027.
[49] D.D. Doneva, L.G. Collodel, C.J. Krüger, S.S. Yazadjiev, Eur. Phys. J. C 80 (12) (2020) 1205.
[50] D.D. Doneva, S.S. Yazadjiev, Phys. Rev. D 103 (6) (2021) 064024.
[51] C.A.R. Herdeiro, E. Radu, N. Sanchis-Gual, J.A. Font, Phys. Rev. Lett. 121 (10) (2018) 101102.
[52] Y.S. Myung, D.C. Zou, Eur. Phys. J. C 79 (3) (2019) 273.
[53] M. Boskovic, R. Brito, V. Cardoso, T. Ikeda, H. Witek, Phys. Rev. D 99 (3) (2019) 035006.
[54] Y.S. Myung, D. Zou, Phys. Lett. B 790 (2019) 400–407.
[55] P.G.S. Fernandes, C.A.R. Herdeiro, A.M. Pombo, E. Radu, N. Sanchis-Gual, Class. Quantum Gravity 36 (13) (2019) 134002;
P.G.S. Fernandes, C.A.R. Herdeiro, A.M. Pombo, E. Radu, N. Sanchis-Gual, Class. Quantum Gravity 37 (4) (2020) 049501, Erratum.
[56] Y. Brihaye, B. Hartmann, Phys. Lett. B 792 (2019) 244–250.
[57] Y.S. Myung, D.C. Zou, Eur. Phys. J. C 79 (8) (2019) 641.
[58] D. Astefanesei, C. Herdeiro, A. Pombo, E. Radu, J. High Energy Phys. 10 (2019) 078.
[59] R.A. Konoplya, A. Zhidenko, Phys. Rev. D 100 (4) (2019) 044015.
[60] P.G.S. Fernandes, C.A.R. Herdeiro, A.M. Pombo, E. Radu, N. Sanchis-Gual, Phys. Rev. D 100 (8) (2019) 084045.
[61] D.C. Zou, Y.S. Myung, Phys. Rev. D 100 (12) (2019) 124055.
[62] Y. Brihaye, C. Herdeiro, E. Radu, Phys. Lett. B 802 (2020) 135269.
[63] D. Astefanesei, J.L. Blázquez-Salcedo, C. Herdeiro, E. Radu, N. Sanchis-Gual, J. High Energy Phys. 07 (2020) 063.
[64] J.L. Blázquez-Salcedo, C.A.R. Herdeiro, J. Kunz, A.M. Pombo, E. Radu, Phys. Lett. B 806 (2020) 135493.
[65] J.L. Blázquez-Salcedo, C.A.R. Herdeiro, S. Kahlen, J. Kunz, A.M. Pombo, E. Radu, Eur. Phys. J. C 81 (2) (2021) 155.
[66] J.L. Blázquez-Salcedo, S. Kahlen, J. Kunz, Symmetry 12 (12) (2020) 2057.
[67] F.M. Ramazanoğlu, Phys. Rev. D 96 (6) (2017) 064009.
[68] F.M. Ramazanoğlu, Phys. Rev. D 98 (4) (2018) 044013.
[69] F.M. Ramazanoğlu, Phys. Rev. D 99 (8) (2019) 084015.
[70] F.M. Ramazanoğlu, K.İ. Ünlütürk, Phys. Rev. D 100 (8) (2019) 084026.
[71] Z.Y. Fan, J. High Energy Phys. 09 (2016) 039.
[72] J.M.S. Oliveira, A.M. Pombo, Phys. Rev. D 103 (4) (2021) 044004.
[73] R.M. Wald, General Relativity, Chicago Univ. Pr, Chicago, USA, 1984.
[74] J. Lee, R.M. Wald, J. Math. Phys. 31 (1990) 725–743.
[75] R.M. Wald, Phys. Rev. D 48 (8) (1993) 3427–3431.
[76] V. Iyer, R.M. Wald, Phys. Rev. D 50 (1994) 846–864.
[77] K. Hajian, M.M. Sheikh-Jabbari, Phys. Rev. D 93 (4) (2016) 044074.
[78] M. Ghodrati, K. Hajian, M.R. Setare, Eur. Phys. J. C 76 (12) (2016) 701.
[79] K. Hajian, S. Liberati, M.M. Sheikh-Jabbari, M.H. Vahidinia, Phys. Lett. B 812 (2020) 136002.
[80] U. Ascher, J. Christiansen, R.D. Russell, Math. Comput. 33 (146) (1979) 659.